Efficient femtosecond pulse generation using a parabolic amplifier combined with a pulse compressor.

I. Stimulated Raman scattering effects

Daniel B. S. Soh*, Johan Nilsson

Optoelectronics Research Centre, University of Southampton, Southampton, SO17 1BJ, UK

Anatoly. B. Grudinin

Fianium Ltd., 20 Compass Point, Ensign Way, Southampton SO31 4RA, UK

* Corresponding author, tel:+44 23 8059 3143, fax: +44 23 8059 3142, e-mail: dbs@orc.soton.ac.uk

The effects of stimulated Raman scattering on femtosecond pulse generation using a parabolic amplifier and a grating pair compressor are presented. We derive an explicit analytical form for the Stokes pulse evolution. We find that the evolution of the Stokes pulse can be divided into four regimes; small Gaussian Stokes pulse, small asymmetric Stokes pulse, signal depletion, and parabolic Raman pulse. In order to achieve efficient pulse compression, the parabolic amplifier should be operated in the small Stokes pulse regime where the signal pulse is not seriously distorted. We also derive an analytical expression to obtain a critical fiber length for the small Stokes pulse regime. The derived theory is applied to a realistic high power femtosecond pulse generation process through a split-step Fourier numerical simulation. The pulse compression results confirm that our derived critical fiber length leads to the highest peak power and shortest width of compressed pulse.

OCIS codes: 190.4370, 060.5530, 190.5650.

1. INTRODUCTION

In order to achieve high power femtosecond pulses from fiber sources, several schemes have been investigated so far. For instance, it was demonstrated that self-frequency shift resulting from anomalous dispersion combined with amplification generates high power femtosecond Raman solitons with red-shifted wavelength.[1,2] On the other hand, a combination of a parabolic amplifier operating in the normal dispersion and a grating pair pulse compressor can also generate high power femtosecond pulses.[3-7] However, intrinsic problems associated with the latter method are that the parabolic amplification process is limited by the Stokes pulses caused by stimulated Raman scattering and the amplifier gain bandwidth. At high powers, the parabolic signal pulse may trigger the amplification of a Stokes pulse which is $13.2\,THz$ away in frequency. This Stokes wave evolves from the noise in the amplifier and seriously distorts the signal pulse, especially in a high power parabolic pulse system. In addition, in a parabolic pulse system, the spectrum of pulse widens rapidly (e.g., exponentially), and may eventually become larger than the doped-fiber amplifier gain bandwidth. This excessive pulse frequency bandwidth is most severe in the high power regime since the spectral width is also proportional to the parabolic pulse energy. Therefore, we provide an in-depth analysis on these two limiting factors in two parts. In part I, an explicit analytical expressions for the evolutions of Stokes and signal pulses are derived for the first time, which eventually leads to an expression for a critical fiber length within which signal pulse degradation can be avoided. In part II, an analytical expression for the signal pulse is derived in the situation of a finite gain bandwidth of the amplifier.

Regarding the Raman Stokes scattering effect, which is the subject of this part I, it is well demonstrated that the Raman Stokes pulse degrades the parabolic amplification process by extracting energy from the main signal pulse.[8] Unfortunately however, the result presented in

Ref. 8 shows large discrepancy from realistic situations in some cases, due to the approximations made. In dealing with stimulated Raman scattering, it is important to maintain an exact analysis with the least number of assumptions. This is because a small error in the beginning of the propagation causes unacceptable errors in the end due to the high gain of Raman scattering. On the other hand, in order to achieve a short compressed pulse with large peak power, it is critical to maintain the parabolic signal pulse intact since even small distortions of the parabolic pulse degrade the pulse compression efficiency. Since stimulated Raman scattering builds up along the fiber, there naturally follows an upper bound on the fiber length, within which the signal pulse may maintain the parabolic shape. Motivated by these ideas we derive an exact analytical solution for the Stokes pulse as well as the signal pulse. We also present a critical length within which the signal may maintain a parabolic nature.

This article (i.e., part I) is organized as follows. In section 2, the analytical solution for the pulses is derived based on the full Schrödinger equation. The expression for the critical length is also derived and presented in this section. Section 3 compares a numerical simulation based on a split-step Fourier method and the analytical solution. Section 4 describes the effect of stimulated Raman scattering on the pulse compression. Finally a conclusion follows in section 5.

2. ANALYTICAL SOLUTIONS FOR THE STOKES PULSE

In this section, we derive an analytical solution for the Stokes pulse. For this, we introduce the nonlinear Schrödinger equation with different amplification for the signal and Stokes pulses. This is appropriate for doped silica fiber amplifiers since, for example, the center wavelength of the signal pulse of an Yb-doped fiber is usually 1060 nm while that of the Stokes pulse is 1110 nm (440 cm^{-1} apart), where the doped-fiber does not provide the same gain. If we assume a

Lorentzian gain profile for the amplifier, peaked at the center wavelength of the signal, the gain of the signal pulse α_s and that of the Stokes pulse α_r has a relationship of $\alpha_r = \alpha_s / \left[1+(\nu_s - \nu_r)^2 / \Delta\nu_{FWHM}{}^2\right]$. Here $\nu_j\,(j=s,r)$ is the optical center frequency of signal and Stokes pulses and $\Delta\nu_{FWHM}$ is the amplifier gain frequency bandwidth (FWHM). Therefore, the nonlinear Schrödinger equation is slightly modified as follows.[9-10]

$$\frac{\partial\psi_s}{\partial z}+\frac{i}{2}\beta_{2s}\frac{\partial^2\psi_s}{\partial T^2}=i\gamma_s\left[|\psi_s|^2+(2-f_R)|\psi_r|^2\right]\psi_s-\frac{g_s}{2}|\psi_r|^2\psi_s+\frac{\alpha_s}{2}\psi_s, \tag{1}$$

$$\frac{\partial\psi_r}{\partial z}-d\frac{\partial\psi_r}{\partial T}+\frac{i}{2}\beta_{2r}\frac{\partial^2\psi_r}{\partial T^2}=i\gamma_r\left[|\psi_r|^2+(2-f_R)|\psi_s|^2\right]\psi_r+\frac{g_r}{2}|\psi_s|^2\psi_r+\frac{\alpha_r}{2}\psi_r, \tag{2}$$

where ψ_s, ψ_r represent the slowly varying envelopes of the signal and Raman Stokes pulses, β_{2j} the dispersion ($j=s,r$), f_R the fractional contribution of the delayed Raman response to the nonlinear polarization[11] (~ 0.18), γ_j the nonlinear coefficients with the relation[12] $\gamma_s=(\lambda_r/\lambda_s)\gamma_r$, g_j the Raman gain coefficient with the relation[12] $g_s=(\lambda_r/\lambda_s)g_r$, d the walk-off parameter ($d\cong\beta_{2s}\Omega_R$ with $\Omega_R=2\pi\times13.2THz$)[9]. In equations (1) and (2), the third-order dispersion term is neglected for the simplicity of analysis. In conventional fibers with a significant third-order dispersion coefficient, the signal may be distorted once the optical spectrum of the signal covers a large spectral region. Therefore, the validity of our analysis is confined to cases when the third-order dispersion is negligible. A fiber with significant third-order distortion is not suitable for parabolic pulse amplification, since it leads the resulting amplitude distortions preventing efficient generation of femtosecond pulses. We proceed with two different regimes for small and large Stokes pulses.

A. Small Stokes Pulse Regime

For the small Stokes pulse case, it is conventional to ignore the cross products terms $|\psi_r|^2\psi_s$ in equation (1). Then, we get back to the conventional parabolic amplification equation and the differential equations (1) and (2) approximate into

$$\frac{\partial\psi_s}{\partial z}+\frac{i}{2}\beta_{2s}\frac{\partial^2\psi_s}{\partial T^2}=i\gamma_s|\psi_s|^2\psi_s+\frac{\alpha_s}{2}\psi_s, \tag{3}$$

$$\frac{\partial\psi_r}{\partial z}-d\frac{\partial\psi_r}{\partial T}+\frac{i}{2}\beta_{2r}\frac{\partial^2\psi_r}{\partial T^2}=\left\{i\gamma_r(2-f_R)+\frac{g_r}{2}\right\}|\psi_s|^2\psi_r+\frac{\alpha_r}{2}\psi_r. \tag{4}$$

Equation (3) has an asymptotic solution given by[3-5]

$$\psi_s=A_0\exp\left(\frac{\alpha_s}{3}z\right)\sqrt{1-\frac{T^2}{T_p^2(z)}}\exp\left[i\left\{\phi_0+\frac{\alpha_s}{12\beta_2}\left(T_p^2(z)-2T^2\right)\right\}\right], \tag{5}$$

for $|T|<T_p(z)$ and, otherwise, 0. Here, $A_0=\left(\alpha_s U_{in}/\sqrt{\gamma_s\beta_{2s}/2}\right)^{1/3}/2$, $T_p(z)=B\exp(\alpha_s z/3)$ where $B=6(A_0/\alpha_s)\sqrt{\gamma_s\beta_{2s}/2}$, and ϕ_0 is a constant. The validity of the asymptotic solution in equation (5) is in fact limited to the case where the spectral bandwidth of the signal pulse is well within that of the amplifier gain bandwidth, the details of which will be described in part II. If we assume the slowly varying envelope approximation in equation (4), which is conventional,[13-16] the second time derivative term is ignored and equation (4) can be exactly solved. By introduction of a new variable $u=z-T/d$, it is straightforward to verify that the following is a solution for equation (4):

$$\psi_r(z,T)=\psi_r(0,T+zd)\exp\left[\frac{\alpha_r}{2}z+\left\{\frac{g_r}{2}+i\gamma_r(2-f_R)\right\}\phi(z,T)\right], \tag{6}$$

where

$$\phi(z,T)=\int_0^z A_0^2\exp\left(\frac{2\alpha_s}{3}z'\right)f(z,z',T)dz', \tag{7}$$

and

$$f(z',z,T)=\begin{cases}1-(T+zd-z'd)^2/T_p^2(z'), & |T+zd-z'd|<T_p(z')\\ 0, & \text{otherwise}\end{cases}. \tag{8}$$

In equation (6), the initial condition $\psi_r(0,T)$ for the Raman Stokes pulse can be fictitiously chosen[17] as $\psi_r(0,T)=\sqrt{P_{r0}}$ where $P_{r0}=h\nu_r B_{eff}$ is the equivalent input power and $B_{eff}=\left[\pi/\left(4I_0L_{eff}g_R\right)\right]^{1/2}\Delta\nu_{FWHM}$ is the effective bandwidth of the spontaneous Raman scattering assuming a Lorentzian gain profile. Here, I_0 is the input signal pulse peak intensity, $L_{eff}=[\exp(\alpha_s L)-1]/\alpha_s$, and $\Delta\nu_{FWHM}$ is the gain bandwidth of the amplifier.

It is worth noting here that the approximate results in Ref. 8 are based on the assumption that $T_p(z')$ in the condition $|T+zd-z'd|<T_p(z')$ may be replaced by $T_p(z)$ in equation (8). However, we have found that this approximation leads to a serious calculation error in some cases, which will be presented in section 3. The calculation error is due to the exponential nature of the solution, which means that a small error in the integrand of equation (7) is amplified through the exponential integration. Therefore, we derived an exact analytical form of the integral in equation (7). For readability, we present here only the final results. The details of the

derivation can be found in appendix A. The final solution for the Stokes pulse is given as follows: We denote the peak intensity of the Stokes pulse as P_r^{peak} and the time at which the peak pulse occurs as T_0. In appendix A it is shown that the strong Raman scattering effect occurs only for $z < z_S$ where $z_S = 3\ln\left(d/2A_0\sqrt{\gamma_s\beta_{2s}/2}\right)/\alpha_s$. For the case $z > z_S$, the Stokes pulse does not grow any more since the Stokes pulse have already 'walked off' completely from the signal as is explained in appendix A. In this case, the Stokes pulse experiences normal dispersion with gain and behaves as a self-similar parabolic pulse. Of course, our primary concern is in the regime where $z \le z_S$, in which the Stokes pulse still grows fast. Then, the analytical solutions in this regime are

(case I) $z < \dfrac{2B}{d}$ (Gaussian Stokes pulse regime):

$$\begin{cases} \psi_r(z,T) = \sqrt{P_{r0}}\exp\left[\dfrac{\alpha_r}{2}z + \left(\dfrac{g_r}{2} + i\gamma_r(2-f_R)\right)\left\{\dfrac{3A_0^2}{2\alpha_s B^2}\left[T_p^2(z) - T_p^2(0)\right] - \dfrac{d^2z^3A_0^2}{12B^2} + \dfrac{zA_0^2}{B^2}\left(T + \dfrac{1}{2}zd\right)^2\right\}\right], \\ P_r^{peak}(z) = P_{r0}\exp\left[\alpha_r z + g_r A_0^2\left\{\dfrac{3}{2\alpha_s B^2}\left[T_p^2(z) - T_p^2(0)\right] - \dfrac{d^2z^3}{12B^2}\right\}\right], \\ T_0(z) = -\dfrac{zd}{2}. \end{cases} \tag{9}$$

(case II) $z \ge \dfrac{2B}{d}$ (Asymmetric Stokes pulse regime):

$$\begin{cases} \psi_r(z,T) = \sqrt{P_{r0}}\exp\left[\dfrac{\alpha_r}{2}z + \left(\dfrac{g_r}{2} + i\gamma_r(2-f_R)\right)\dfrac{A_0^2}{B^2}\left\{\dfrac{3}{2\alpha_s}\left[T_p^2(z) - T_p^2(z_{\min})\right] - \dfrac{1}{3d}\left[T^3 - T_p^3(z_{\min})\right]\right\}\right], \\ P_r^{peak}(z) = P_{r0}\exp\left[\alpha_r z + \dfrac{3A_0^2 g_r}{2\alpha_s B^2}\left\{T_p^2(z) - T_0^2(z)\left(1 - \dfrac{4\alpha_s}{9d}T_0(z)\right)\right\}\right], \\ T_0(z) = -\dfrac{3d}{2\alpha_s}W\left(\dfrac{2\alpha_s}{3d}T_p(z)\right). \end{cases} \tag{10}$$

In equation (10), $z_{\min}$ is a function of z,T and describes the longitudinal position where the Stokes pulse starts to interact with the signal pulse. Once the Stokes pulse enters into the asymmetric Stokes pulse regime, $z_{\min}$ becomes positive for some region of time T due to the effects of the pulse width broadening combined with the walk-off between pulses. Especially, the temporal position for the peak of the Stokes pulse belongs to this region of time. In appendix A, $z_{\min}$ is derived as

$$z_{\min}(z,T) = \frac{-3}{\alpha_s d}W\left[\frac{\alpha_s d}{3d}\exp\left\{\frac{\alpha_s}{3d}(T+zd)\right\}\right] + \frac{1}{d}(T+zd). \tag{11}$$

In equations (10) and (11), W is the well-known Lambert W-function.[18] Its definition and properties are given in appendix C.

From equations (9) and (10), we can tell that for the Gaussian Stokes pulse regime ($z < 2B/d$), the Stokes pulse is a symmetric Gaussian, whose pulse width gradually reduces as it propagates. Then, the pulse width reaches its minimum at the point $z = 2B/d$, and gradually increases. Thereafter, the pulse shape becomes asymmetric due to the nature of $z_{\min}$. This

phenomenon is very similar to the case of an anomalous dispersion Raman Stokes pulse as in Ref. 13-16. On the other hand, the time T_0 at which the peak power occurs moves towards the negative T direction with a constant speed in the Gaussian Stokes pulse regime and the moving speed gradually reduces once the pulses enter the asymmetric Stokes pulse regime. This is due to the property of the Lambert W-function as in appendix C. Regarding the peak Stokes pulse power P_r^{peak}, in general it increases doubly exponentially with the propagation distance due to the exponential increase of $T_p(z)$. Please note that the increase rate of $T_p(z)$ is much larger than $T_0(z)$ in equation (10).

B. Large Stokes Pulse Regime

We now proceed to the large Stokes pulse regime where the Stokes pulse becomes large enough to deplete the signal pulse. Then, the assumption that the signal is a parabolic pulse is no more valid. Furthermore, the small Stokes pulse assumption is no more valid, either. Here, we consider a Stokes pulse 'large' when $|\psi_r|^2 > \alpha_s / g_s$. Once the Raman Stokes pulse grows to this level, the signal pulse itself becomes depleted fast due to the doubly exponential growth of the Raman Stokes pulse. It is reasonable to define the large Stokes pulse regime as $z > z_0$ where z_0 satisfies $P_r^{peak}(z_0) = 2\alpha_s / g_s$. The factor 2 in this definition is intended to represent the idea that a significant part of the Stokes pulse should exceed α_s / g_s, not just the peak. Furthermore, we call this z_0 the 'critical length'. The value of z_0 can be found from equation (10) by numerically solving

$$P_{r0} \exp\left[\alpha_r z_0 + \frac{3A_0^2 g_r}{2\alpha_s B^2}\left\{T_p^2(z_0) - T_0^2(z_0)\left(1 - \frac{4\alpha_s}{9d} T_0(z_0)\right)\right\}\right] = \frac{2\alpha_s}{g_s}, \tag{12}$$

where $T_0(z_0)$ is defined in equation (10). Once z_0 is found, $\psi_s(z_0,T)$ can be obtained from equation (5) and $\psi_r(z_0,T)$ from equation (10). Then, it follows that equations (9) and (10) are valid only for $z < z_0$.

If the Stokes pulse peak power enters this large Stokes pulse regime, the Raman gain term in equations (1) and (2) becomes larger than that of the amplifier gain. On the other hand, due to the finite pulse width of the Stokes pulse, there are two time sections of the signal pulse, distinguished by whether there is a strong Raman gain due to strong overlap between signal and Stokes pulse. Those two time sections are approximated as $\Theta_1 = [-2T_{r0}(z_0)+T_0(z_0),\ 2T_{r0}(z_0)+T_0(z_0)]$ for the strong overlap section and $\Theta_2 = [2T_{r0}(z_0)+T_0(z_0),\ T_p(z_0)]$. Here, $T_{r0}(z_0)$ is the pulse width (FWHM) of the Stokes pulse at $z = z_0$ which can be found numerically by equation (12) and $T_0(z_0)$ is the time when the peak intensity occurs as described above. Then, for the time band of Θ_1, the Schrödinger equation can be approximated by the slowly varying envelope approximation as[13-16]

$$\frac{\partial \psi_s}{\partial z} = i\gamma_s\left[|\psi_s|^2 + (2-f_R)|\psi_r|^2\right]\psi_s - \frac{g_s}{2}|\psi_r|^2\psi_s, \tag{13}$$

$$\frac{\partial \psi_r}{\partial z} - d\frac{\partial \psi_r}{\partial T} = i\gamma_r\left[|\psi_r|^2 + (2-f_R)|\psi_s|^2\right]\psi_r + \frac{g_r}{2}|\psi_s|^2\psi_r, \tag{14}$$

with the initial condition of $\psi_s(z_0,T)$ and $\psi_r(z_0,T)$ where $T \in \Theta_1$. On the other hand, for Θ_2 the Schrödinger equation is reduced to the parabolic differential equation without any Stokes effect:

$$\frac{\partial \psi_s}{\partial z} + i\beta_2\frac{\partial^2 \psi_s}{\partial T^2} = i\gamma_s|\psi_s|^2\psi_s + \frac{\alpha_s}{2}\psi_s. \tag{15}$$

Therefore, for $T \in \Theta_2$, ψ_s is obtained as a parabolic pulse according to equation (5).

In fact, the coupled differential equations in equation (13) and (14) are well known in the literature. We provide here the final analytical solutions (for a derivation, see the appendix B). For $T \in \Theta_1$,

$$\begin{cases} |\psi_s(z,T)|^2 = \dfrac{d|\psi_s(z_0,T)|^2 L(T)}{H(z,T)}, \\ |\psi_r(z,T)|^2 = \dfrac{d|\psi_r(z_0,T+d(z-z_0))|^2 L(T+(z-z_0)d)}{H(z,T)}, \end{cases} \tag{16}$$

where

$$\begin{cases} H(z,T) = F(T) + G(T+d(z-z_0)), \\ L(T) = \exp\left\{\dfrac{1}{d}\int_0^T \left[g_r|\psi_s(z_0,T')|^2 + g_s|\psi_r(z_0,T')|^2\right]dT'\right\}, \\ F(T) = g_r \int_0^T |\psi_s(z_0,u)|^2 L(u)du, \\ G(T) = g_s \int_0^T |\psi_r(z_0,u)|^2 L(u)du. \end{cases} \tag{17}$$

Once the signal becomes depleted to the point where the Raman gain becomes negligible, the Stokes pulse follows a differential equation

$$\frac{\partial \psi_r}{\partial z} + i\beta_{2r}\frac{\partial^2 \psi_r}{\partial T^2} = i\gamma_r|\psi_r|^2\psi_r + \frac{\alpha_r}{2}\psi_r, \tag{18}$$

which is again a parabolic differential equation. Therefore, from the point where the signal pulse intensity $|\psi_s|^2$ becomes less than α_r / g_r, the Stokes pulse transforms into a parabolic pulse and propagates according to the parabolic nature. For convenience, we define a length z_1 through

$\left|\psi_s\left(z_1, T_0(z_1)\right)\right|^2 = \alpha_r / g_r$ where $T_0(z_1)$ is the time when the Stokes pulse reaches its peak power. The length z_1 represents the propagation distance where the depleting Raman gain in equation (1) exceeds that of the amplifier gain at some time position in signal pulse. The value of found z_1 can be solved numerically using equations (16)-(17). Then, once the pulse passes z_1, the Stokes pulse itself evolves parabolically. Therefore, the solution of ψ_r is obtained through the parabolic solution in equation (5) with the 'initial' condition of $\psi_r(z_1, T)$.

In summary, we divided the evolution of the Stokes pulse into four regimes; (1) small Gaussian Stokes pulse regime ($z < 2B/d$), (2) small asymmetric Stokes pulse regime ($2B/d \le z < z_0$), (3) signal depletion regime ($z_0 \le z < z_1$), and finally (4) parabolic Stokes pulse regime ($z < z_1$). The lengths z_0, z_1 can be obtained through the previous analytical solutions. We also derived analytical solutions for the signal pulse in the different regimes.

3. NUMERICAL SIMULATIONS

In order to verify the validity of our analytical solutions for the Raman Stokes pulse, we simulated the nonlinear Schrödinger equation in equations (1) and (2), using the trapezoidal split-step Fourier method.[4] For simulations, we took typical parameters for a $27\ \mu m$ mode-field diameter Yb-doped silica fiber, i.e., $\beta_2 = 20\, ps^2 km^{-1}$, $\gamma_s = 0.27\, W^{-1} km^{-1}$, $g_s = 0.155\, W^{-1} km^{-1}$. The signal wavelength is $1.06\ \mu m$. Therefore, the Stokes pulse center wavelength is $1.11\ \mu m$ and the corresponding values of γ_r and g_r are $0.257\, W^{-1} km^{-1}$ and $0.148\, W^{-1} km^{-1}$, respectively. The seed signal is assumed to be a 533 fs (FWHM) Gaussian pulse with energy 1 nJ. For the gain bandwidth of the Yb-doped fiber amplifier, we choose $\Delta\nu_{FWHM} = 10\ THz$. For the fictitious

Raman seed calculation, we picked $g_R = 0.94\times10^{-13}\ m^{-1}W^{-1}$.[8] The signal gain is selected as 4 dB/m, which makes the Stokes pulse gain 2.54 dB/m according to the Lorentzian lineshape of gain profile with bandwidth of $\Delta\nu_{FWHM} = 10\ THz$. The fiber length is 8 m. With these parameters, we calculate the 'strong Raman interaction length' $z_S = 3\ln\left(d/2A_0\sqrt{\gamma_s\beta_{2s}/2}\right)/\alpha_s$ as 8.16 m. Therefore, our entire fiber length falls into this strong Raman interaction regime. The Gaussian Stokes pulse regime is $z < 2B/d = 0.53$ m from analysis. The signal depletion starts from z_0, which is calculated from equation (12) to 7.23 m. Therefore, equation (9) and (10) are valid only for $z < 7.23$ m and this is the small Stokes pulse regime. The parabolic Stokes pulse distance z_1 was calculated through numerical analysis to 7.57 m.

Fig. 1 shows the numerical simulation results for the propagation of the signal and Stokes pulses. From the graphs, we can clearly see three regimes, although maybe not four; small Stokes pulse regime, signal depletion regime, and finally, parabolic Stokes pulse regime. We cannot clearly discriminate between the small Gaussian Stokes pulse regime and the small asymmetric Stokes pulse regime. We can see several features in each section. First, in the small Stokes pulse regime the signal pulse is a typical parabolic pulse while the Stokes pulse grows almost as a double exponential. Second, when the propagation reaches ~7.2 m, the signal pulse starts being depleted, which coincides with theoretical 'critical length' of $z_0 = 7.23$ m. Please note that there are two time sections of the signal pulse, one of which shows signal depletion and the other of which is not depleted and propagates as part of parabolic pulse. This is due to the overlap between signal and Stokes pulse as is explained by theory. According to theory, the center of the signal depletion region should be $T = T_0(z_0)$, which is calculated from equation (10) as $-1.94\ ps$. This value is close to -1.89 ps from the numerical simulation. The signal depletion

takes place in a relatively short distance of 0.34 m, which is calculated from equation (16) and the value of z_1. Finally, after 7.57 m of propagation, the Stokes pulse develops parabolically as can be seen in Fig. 1(b). Please note that the growth of the Stokes parabolic pulse width is very fast because of the large 'initial' pulse energy of the Stokes pulse (at $z = 7.57$ m) and because the parabolic pulse width T_p is proportional to $U_{in}^{1/3}$.

In Fig. 2, the peak powers of the signal and Stokes pulses are shown. From the figure., it is apparent that the analytical solution for the Stokes pulse (O mark) is almost indistinguishable from the numerical solution (solid line). On the other hand, the approximation that $T_p(z')$ is replaced by $T_p(z)$ in equation (8), which is the key approximation in Ref. 8 led to huge calculation errors as is shown (dotted line). This follows from that $f(z, z', T)$ can be negative due to this replacement approximation, which eventually caused a significantly smaller value of ϕ, which again affected ψ_r in an exponential way. For each region, the analytical solution was calculated from equation (9) (region I), equation (10) (region II), equation (16)-(17) (region III), and finally equation (18) (region IV). The small error in region III and IV stems from the approximation in equation (13)-(14), in which zero amplifier gain is assumed. In reality, there still exists (Yb-induced) amplifier gain, however small it is, which causes the analytical solution to be slightly smaller than the numerical solution based on the full Schrödinger equation (equations (1) and (2)).

Fig. 3 shows the time position $T_0(z)$ in equations (9) and (10) where the peak power of the Stokes pulse reaches its maximum. The division between region I and II is clearly shown in Fig. 3. In region I (small Gaussian stokes pulse regime), both the numerical solution and analytical solutions move in the negative T direction with constant speed. Once the pulse enters

region II (small asymmetric stokes pulse regime), it shows a complicated behavior, which is well described by equation (10). The analytical solution (O mark) slightly differs from the numerical solution (solid line) especially in the beginning of region I. This is due to the fact that there exists a finite propagation length where the Gaussian initial signal pulse transforms and converges to the parabolic pulse. Then, the numerical solution gradually converges to the analytical solution in region II. In the last part of region II, the numerical solution starts to differ from the analytical solution due to signal depletion. Nevertheless, the numerical simulation clearly shows two different regimes, which is well explained by dividing regions as in equations (9) and (10).

4. THE EFFECT OF RAMAN SCATTERING ON PULSE COMPRESSION

There are a number of methods to compress a parabolic signal pulse. For instance, fiber gratings can compress the pulse[17] and a single-mode fiber itself can compress the pulse, too[18]. A simple bulk grating pair can also compress the pulse quite efficiently[6,19-21], and is especially convenient for simulation purposes. For this, we introduce a phase compensation term in a grating pair[19-21]

$$\phi_c(\omega) = -a_c(\omega-\omega_0)^2\left\{1-\beta_c\frac{\omega-\omega_0}{\omega_0}\right\}, \tag{19}$$

where $a_c = b_0\lambda_0^3/\left(4\pi c^2 d_0^2\cos^2\gamma'\right)$, b_0 the distance between two gratings, λ_0 the central wavelength, d_0 the spacing between grating grooves, and γ' the angle between the normal and diffracted beam at λ_0. β_c is the third order dispersion coefficient given by $\beta_c = (1-\sin\gamma\sin\gamma')/\cos^2\gamma'$, where γ is the angle between the incident beam and the grating normal. The angle γ' is calculated with the grating equation $\gamma' = \sin^{-1}(\sin\gamma - \lambda_0/d)$.[11] For

simulation purposes, we took as an example a grating from Optometrics with 600 grv/mm blazed at 1 μm. The incident angle is assumed to be 17°. For each case of pulse compression, we use the optimized grating distance which provides the maximum peak power in the compressed pulse. For instance, Fig. 4 shows the compression results from the signal pulse output at $z = 5$ m. In this case, the peak power of the compressed pulse is 1.12 MW and the pulse width is 88 fs with an optimum grating distance of 6.57 cm. Due to the third order dispersion of the compressor, the compressed pulse has tails.

Fig. 5 shows the optimum compression results for the signal pulse *vs.* propagation distance. The graph clearly shows that the compressed signal pulse reaches its highest peak power of 8.38 MW as well as its minimum duration of 64 fs for $z = 7.2\ \mathrm{m} (\cong z_0)$. As is apparent from Fig. 1, the signal pulse experiences strong depletion beyond $z = 7.2$ m, which again degrades the pulse compression. While the spectral width of a parabolic pulse increases exponentially, and the pulse therefore compresses to shorter durations with somewhat longer propagation distance, the fraction of the energy in the compressed pulse becomes smaller as the pulse distorts.

Thus, for efficient pulse compression, the signal pulse must not be distorted by the Raman Stokes pulse. The critical length z_0 (in our case 7.2 m) characterizes the maximum amplifier length that allows efficient pulse compression.

5. CONCLUSIONS

We have derived an analytical solution for the Raman-scattered Stokes pulse associated with parabolic amplification. It is shown that there are four regimes; (1) small Gaussian Stokes pulse regime, (2) small asymmetric Stokes pulse regime, (3) signal depletion regime, and (4) parabolic

Stokes pulse regime. We have demonstrated the validity of our analytical solution by comparing it to a numerical simulation based on a trapezoidal split-step Fourier transform. The comparison shows that our analytical solution is accurate. We also investigated the effect of Raman scattering on pulse compression. The results clearly show that the parabolic amplifier should be operated in the small Stokes pulse regime where the signal pulse remains intact. Once the pulse propagates further than the critical length z_0, which is a solution of equation (12), stimulated Raman scattering begins to deplete and distort the signal pulse, resulting in degraded pulse compression. Therefore, in order to achieve the shortest pulse with the largest peak power, one should limit the fiber length below the critical length z_0.

APPENDIX A: DERIVATION OF ANALYTICAL SOLUTIONS FOR SMALL STOKES PULSE REGIME

We start with equations (3) and (4). The boundary condition in equation (8) implies that equation (7) is integrated in the range of $z' \in [\max\{0, z_{\min}\}, \min\{z, z_{\max}\}]$ where $z_{\min}, z_{\max}$ satisfy

$$\begin{cases} z_{\max} d - T_p(z_{\max}) = T + zd, \\ z_{\min} d + T_p(z_{\min}) = T + zd. \end{cases} \tag{A1}$$

Now, we confine the time T of concern as $T > -T_p(z)$ since the signal and Stokes pulse interact only in this region. Then, we have

$$z_{\max} d - T_p(z_{\max}) > zd - T_p(z). \tag{A2}$$

Please note that the function $h(z)=zd-T_p(z)$ is monotonically increasing if and only if $z \le 3\ln(3d/\alpha_s B)/\alpha_s$. In this case, inequality in (A2) implies $z_{max} > z$ so that the integration in equation (7) terminates at z. Otherwise, for some point in the range of interest $T > -T_p(z)$, the integral termination becomes z_{max} which is smaller than z, which in turn has less integral weight $\exp(\alpha_s z'/3)$ implying weaker interaction between signal and Stokes pulse. Once, the pulse passes the point $z = 3\ln(3d/\alpha_s B)/\alpha_s$, it is expected that the Raman interaction gradually wears out so that the Stokes pulse growth rate reduces and eventually stops. Therefore, $z_S = 3\ln(3d/\alpha_s B)/\alpha_s$ is the critical point for strong Raman scattering and we call this point a 'strong Raman interaction characteristic length'. Our primary concern in this paper lies in the regime where the signal and Stokes pulse interact strongly and therefore, we derive all the following equations in the regime within the Raman interaction characteristic length. Then, the equation (7) can be evaluated as follows:

$$\phi(z,T) = A_0^2\left[\frac{3}{2\alpha_s}\left\{\exp\left(\frac{2\alpha_s z}{3}\right)-\exp\left(\frac{2\alpha_s a}{3}\right)\right\}+\frac{1}{3dB^2}\left\{T^3-(T+(z-a)d)^3\right\}\right], \qquad \text{(A3)}$$

where $a = \max\{0, z_{min}\}$. Our objectives in this analytical derivation are, first, to find the peak Stokes pulse intensity and, second, the time T_0 at which this peak occurs. Hence, we find T_0 where $\partial\psi_r(z,T_0)/\partial T = 0$ which is a sufficient and necessary condition for $\partial\phi(z,T_0)/\partial T = 0$. In case of $z_{min} < 0$, the time derivative of equation (A3) easily gives $T_0 = -zd/2$ and the peak power as in equation (9). Please note that by equation (A1),

$$z_{min}(z,T) = z+\frac{T}{d}-\frac{3}{\alpha_s}W\left[\frac{\alpha_s B}{3d}\exp\left(\frac{\alpha_s(T+zd)}{3d}\right)\right], \qquad \text{(A4)}$$

Then, $z_{\min}(z,T_0)$ is given by

$$z_{\min}(z,T_0)=\frac{z}{2}-\frac{3}{\alpha_s}W\left(\frac{\alpha_s B}{3d}\exp\left(\frac{\alpha_s z}{6}\right)\right). \tag{A5}$$

which is negative if and only if $z<2B/d$. Therefore, equation (9) is valid for $z<2B/d$. Consequently, in this case, we have

$$\phi(z,T)=A_0^2\left[\frac{3}{2\alpha_s}\left\{\exp\left(\frac{2\alpha_s z}{3}\right)-1\right\}+\frac{1}{3dB^2}\left\{T^3-(T+zd)^3\right\}\right], \tag{A6}$$

which yields equation (9).

If $z_{\min}$ is positive, equation (A3) yields

$$\phi(z,T)=\frac{A_0^2}{B^2}\left[\frac{3}{2\alpha_s}\left\{T_p^2(z)-T_p^2(z_{\min})\right\}+\frac{1}{3d}\left\{T^3-T_p^3(z_{\min})\right\}\right]. \tag{A7}$$

By differentiating equation (A7) with respect to T and using $\partial T_p(z_{\min})/\partial T=(\alpha_s/3)(\partial z_{\min}/\partial T)T_p(z_{\min})$ and the time derivative $\partial z_{\min}/\partial T$ from equation (A1) yields

$$T_0=-T_p(z_{\min}(z,T_0))=-\frac{1}{2}d\{z-z_{\min}(z,T_0)\}. \tag{A8}$$

By noting that $z_{\min}(z,T)$ is given from equation (A4), it is straightforward to confirm that the following expression for T_0 solves equation (A8):

$$T_0=-\frac{3d}{2\alpha_s}W\left(\frac{2\alpha_s}{3d}T_p(z)\right). \tag{A9}$$

This solution makes $z_{\min}(z,T_0)$ positive. Now, with the help of equation (A8), equation (A7) yields

$$\phi(z,T_0)=\frac{3A_0^2}{2\alpha_s B^2}\left\{T_p^2(z)-T_0^2(z)\left(1-\frac{4\alpha_s}{9d}T_0(z)\right)\right\}. \tag{A10}$$

On the other hand, $\psi_r(z,T)$ is obtained by putting equation (A7) into equation (6). In summary, equation (9) and equation (10) are derived.

APPENDIX B: DERIVATION OF ANALYTICAL SOLUTIONS IN THE SIGNAL DEPLETION REGIME

We follow a procedure to that in Ref. 16. We introduce new variables $x=T$, $y=T+dz$. Then, equation (13) and (14) transform into

$$\frac{\partial\psi_s}{\partial y}=i\frac{\gamma_s}{d}\left[|\psi_s|^2+(2-f_R)|\psi_r|^2\right]\psi_s-\frac{g_s}{2d}|\psi_r|^2\psi_s, \tag{B1}$$

$$\frac{\partial\psi_r}{\partial x}=-i\frac{\gamma_r}{d}\left[|\psi_r|^2+(2-f_R)|\psi_s|^2\right]\psi_r-\frac{g_r}{2d}|\psi_s|^2\psi_r. \tag{B2}$$

Letting

$$\begin{cases}\psi_s(x,y)=I_s^{1/2}(x,y)\exp[i\theta_s(x,y)],\\ \psi_r(x,y)=I_r^{1/2}(x,y)\exp[i\theta_r(x,y)],\end{cases} \tag{B3}$$

where $I_{j=s,r}$ and $\theta_{j=s,r}$ are real variables, gives four differential equations:

$$\begin{cases} \dfrac{\partial I_s}{\partial y}+\dfrac{g_s}{d}I_rI_s=0, \\ \dfrac{\partial I_r}{\partial x}+\dfrac{g_r}{d}I_rI_s=0, \\ \dfrac{\partial \theta_s}{\partial y}=\dfrac{\gamma_s}{d}[I_s+(2-f_R)I_r], \\ \dfrac{\partial \theta_r}{\partial x}=\dfrac{\gamma_r}{d}[I_r+(2-f_R)I_s] \end{cases}, \tag{B4}$$

Then, following a similar method as in Ref. 16, it is straightforward to verify that the following is a solution of the first two equations in (B4):

$$I_s(x,y)=\frac{I_{s0}(x)L(x)d}{H(x,y)}, \tag{B5a}$$

$$I_r(x,y)=\frac{I_{r0}(y)L(y)d}{H(x,y)}, \tag{B5b}$$

where

$$\begin{cases} H(x,y)=F(x)+G(y), \\ L(u)=\exp\left\{\dfrac{1}{d}\int_0^u[g_rI_{s0}(v)+g_sI_{r0}(v)]dv\right\}, \\ F(x)=g_r\int_0^x I_{s0}(u)L(u)du, \\ G(y)=g_s\int_0^y I_{r0}(u)L(u)du. \end{cases} \tag{B6}$$

Here, $I_{s0}(T)=|\psi_s(z_0,T)|^2$ and $I_{r0}(T)=|\psi_r(z_0,T)|^2$ are the initial conditions. It remains to determine z_0 for those initial conditions. We started from the assumption that once $|\psi_r^{peak}|^2>2\alpha/g_r$ holds, equations (1) and (2) reduce to equations (B1) and (B2). Once z_0 is obtained through equation (12), one uses equations (9) and (10) in order to obtain I_{s0} and I_{r0}. On

the other hand, the phase terms are given by equation (A2) and (A4) and can be easily integrated. The final solutions for those phases can be found in Ref. 16, and are not presented here for compactness.

APPENDIX C: LAMBERT W-FUNCTION

The Lambert W-function is extensively used in modern engineering and scientific problems, mostly by fractal researchers. The definition of Lambert W-function is the inverse function of

$$f(W)=W\exp(W). \tag{C1}$$

Therefore, it directly has the property of

$$W(x)\exp[W(x)]=x. \tag{C2}$$

One useful theorem is that the solution of $(a+bx)\exp(cx)=d$ is directly given by $x=W[(cd/b)\exp(ac/b)]/c-a/b$. The Lambert W-function $W(x)$ has a real value for $x\geq -e^{-1}$. Furthermore, for small value ($x<e^{-1}$), it has a Taylor series expansion of

$$W(x)=\sum_{n=1}^{\infty}\frac{(-n)^{n-1}}{n!}x^n. \tag{C3}$$

For convenience, we introduce the graph of Lambert W-function in Fig. 6.

REFERENCES

1. J. P. Gordon, "Theory of the soliton self-frequency shift," Opt. Lett. **11**, 662-664 (1986).
2. D. J. Richardson, V. V. Afanasjev, A. B. Grudinin, and D. N. Payne, "Amplification of femtosecond pulses in a passive, all-fiber soliton source," Opt. Lett. **17**, 1596-1598, 1992.
3. M. E. Fermann, V. I. Kruglov, B. C. Thomsen, J. M. Dudley, and J. D. Harvey, "Self-similar propagation and amplification of parabolic pulses in optical fibers," Phys. Rev. Lett. **84**(26), 6010-6013 (2000).
4. V. I. Kruglov, A. C., Peacock, and J. D. Harvey, "Exact self-similar solutions of the generalized nonlinear Schrödinger equation with distributed coefficients," Phys. Rev. Lett. **90**, 113902 (2003).
5. V. I. Kruglov, A. C., Peacock, J. D. Harvey, and J. M. Dudley, "Self-similar propagation of parabolic pulses in normal-dispersion fiber amplifiers," J. Opt. Soc. Am. B **19**, 461-469 (2002).
6. J. Limpert, T. Schreiber, T. Clausnitzer, K. Zollner, H.-J. Fuchs, E.-B. Kley, H. Zellmer, and A. Tünnermann, "High-power femtosecond Yb-doped fiber amplifier," Opt. Express **10**, 628-638 (2002).
7. C. Finot, G. Millot, S. Pitois, C. Billet, and J. M. Dudley, "Numerical and experimental study of parabolic pulses generated via Raman amplification in standard optical fibers," IEEE J. Sel Topics in Quantum Electron. **10**, 1211-1218, 2004.
8. G. Chang, Al Galvanauskas, H. G. Winful, and T. B. Norris, "Dependence of parabolic pulse amplification on stimulated Raman scattering and gain bandwidth," Opt. Lett. **29**, 2647-2649 (2004).
9. G. P. Agrawal, *Nonlinear fiber optics*, 3rd ed. (Academic Press, New York, 2001).

10. C. Headley and G. P. Agrawal, "Unified description of ultrafast stimulated Raman scattering in optical fibers," J. Opt. Soc. Am. B **13**, 2170-2177 (1996).

11. R. H. Stolen, J. P. Gordon, W. J. Tomlinson, and H. A. Haus, "Raman response function of silica-core fibers," J. Opt. Soc. Am. B **6**, 1159-1166 (1989).

12. M. Kuckartz, R. Schultz, and H. Harde, "Theoretical and experimental studies of the combined self-phase modulation and stimulated Raman-scattering in single-mode fibres," Opt. Quantum Electron. **19**, 237-246 (1987).

13. J. T. Manassa, "Induced phase modulation of the stimulated Raman pulse in optical fibers," Appl. Opt. **26**, 3747-3749 (1987).

14. J. T. Manassa and O. Cockings, "Time-domain characteristics of a Raman pulse in the presence of a pump," Appl. Opt. **26**, 3749-3752 (1987).

15. J. Herrmann and J. Mondry, "Stimulated Raman scattering and self-phase modulation of ultrashort light pulses in optical fibres," J. Modern Opt. **35**, 1919-1932 (1988).

16. D. N. Christodoulides and R. I. Joseph, "Theory of stimulated Raman scattering in optical fibers in the pulse walk-off regime," IEEE J. Quant. Electron. **25**, 273-279 (1989).

17. N. G. R. Broderick, D. Taverner, D. J. Richardson, M. Ibsen, and R. I. Laming, "Optical pulse compression in fiber Bragg gratings," Phys. Rev. Lett. **79**, 4566 (1997).

18. D. Anderson, M. Lisak, and P. Anderson, "Nonlinear enhanced chirp pulse compression in single-mode fibers," Opt. Lett. **10**, 134-136 (1985).

19. E. B. Treacy, "Optical pulse compression with diffraction gratings," IEEE J. Quantum Electron. **QE-5**, 454-458 (1969).

20. W. J. Tomlinson and W. H. Knox, "Limits of fiber-grating optical pulse compression," J. Opt. Soc. Am. B **4**, 1404-1411 (1987).

21. O. E. Martinez, "Grating and prism compressors in the case of finite beam size," J. Opt. Soc. Am. B **3**, 929-934 (1986).

List of figure captions

Fig. 1. Numerical simulation of signal and Stokes pulse propagation in 8 m fiber. (a) Signal pulse, (b) Stokes pulse.

Fig. 2. The peak power of signal pulse (dashed line), numerical simulation of Stokes pulse (solid line), analytical solution (O mark), and the approximation of Ref. 8. The region numbers indicate I: small Gaussian Stokes pulse regime, II: small asymmetric Stokes pulse regime, III: signal depletion regime, and IV: parabolic Stokes pulse regime.

Fig. 3. The time position in relative time coordinate, where the peak power of the Stokes pulse occurs. Numerical solution: solid line. Analytical solution: O mark. The dashed lines represent the signal pulse width $T_p(z)$. The region numbers indicate I: small Gaussian Stokes pulse regime and II: small asymmetric Stokes pulse regime.

Fig. 4. The compressed pulse from the parabolic signal pulse at $z = 5\ m$. (a) The compressed pulse output. (b) The peak power of compressed pulses vs. grating distance.

Fig. 5. Pulse compressor simulation results for the signal pulse vs. propagation distance. The peak powers of the compressed pulses are plotted (dotted line) with the corresponding pulse width (O mark).

Fig. 6. Lambert W-function.

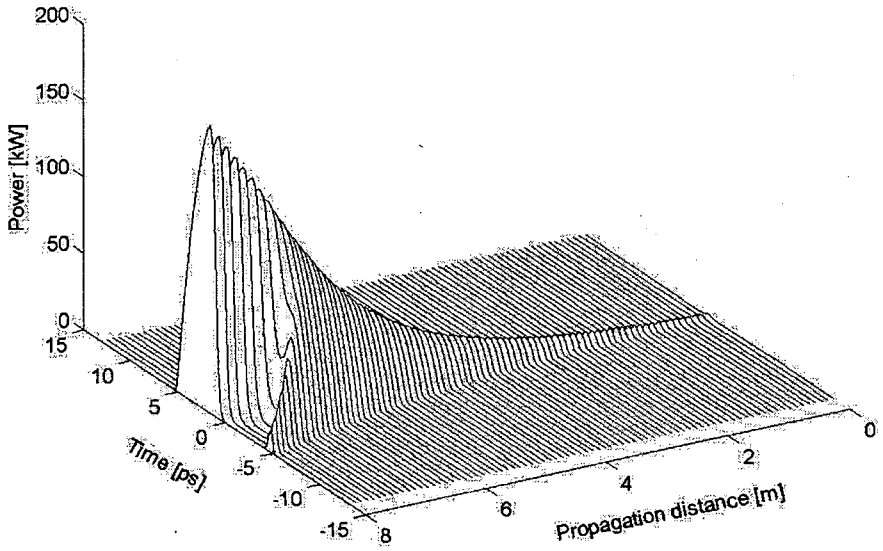

(a)

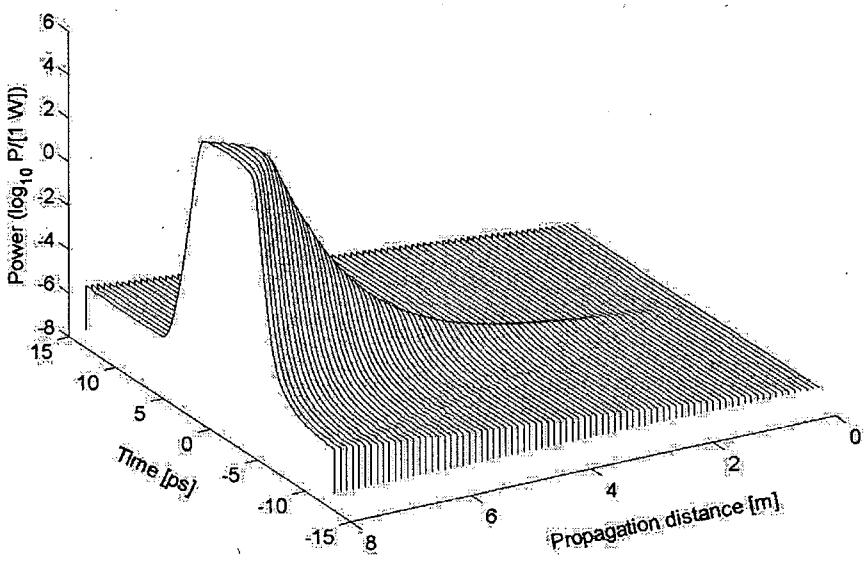

(b)

Figure 1. Numerical simulation of signal and Stokes pulse propagation in 8 m fiber. (a) Signal pulse, (b) Stokes pulse.

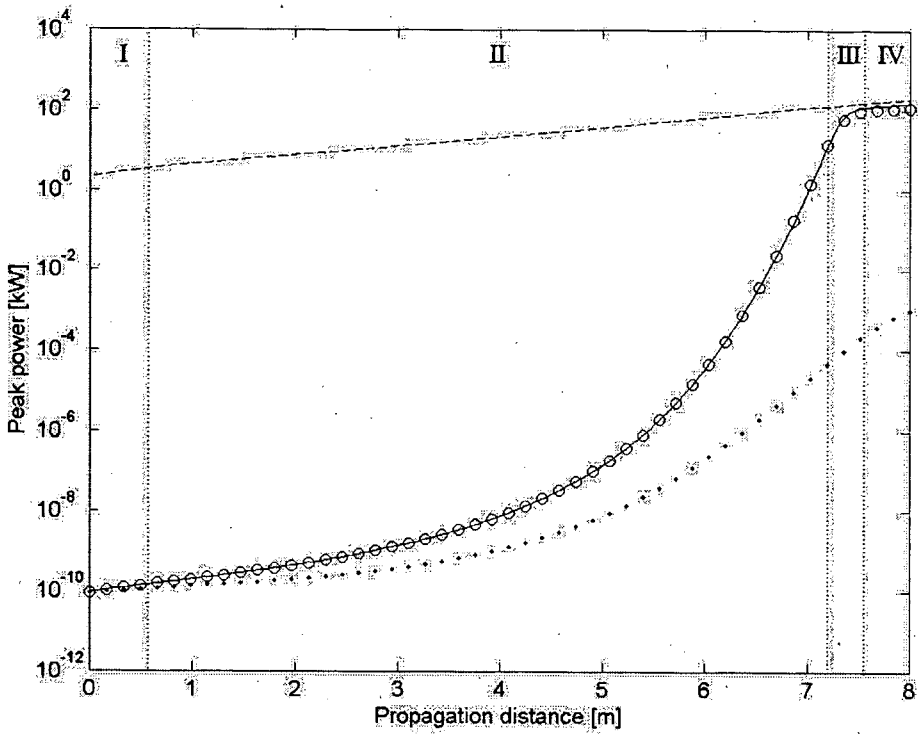

Fig. 2. The peak power of signal pulse (dashed line), numerical simulation of Stokes pulse (solid line), analytical solution (O mark), and the approximation of Ref. 8. The region numbers indicate I: small Gaussian Stokes pulse regime, II: small asymmetric Stokes pulse regime, III: signal depletion regime, and IV: parabolic Stokes pulse regime.

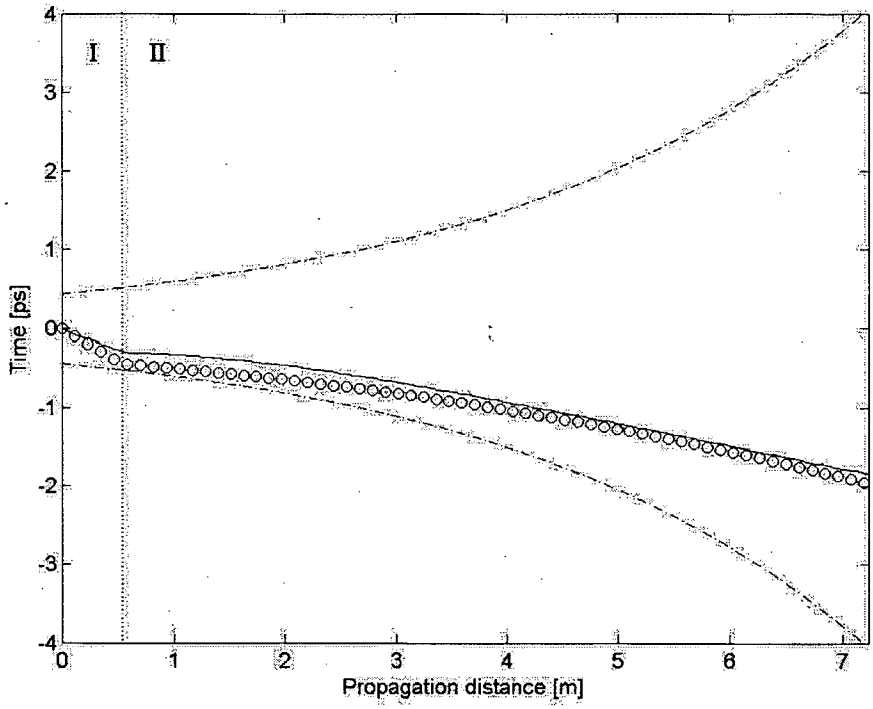

Fig. 3. The time position in relative time coordinate, where the peak power of the Stokes pulse occurs. Numerical solution: solid line. Analytical solution: O mark. The dashed lines represent the signal pulse width $T_p(z)$. The region numbers indicate I: small Gaussian Stokes pulse regime and II: small asymmetric Stokes pulse regime.

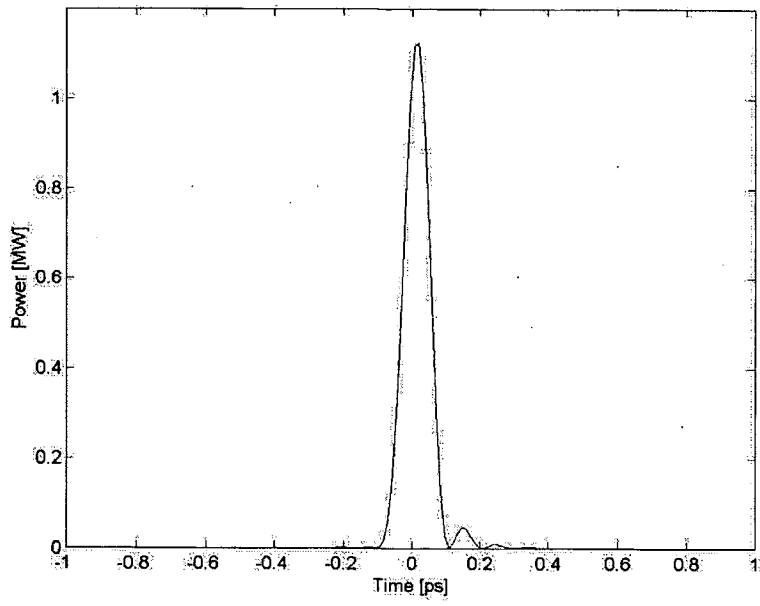

(a)

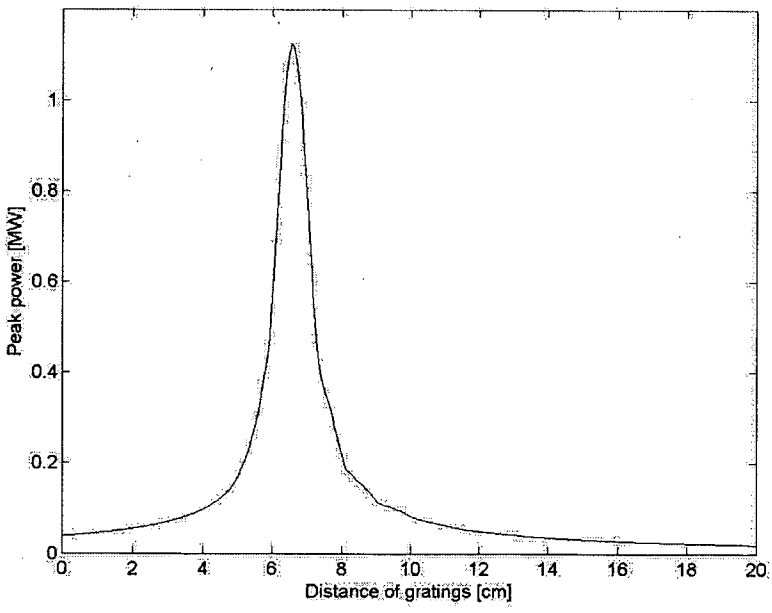

(b)

Fig. 4. The compressed pulse from the parabolic signal pulse at $z = 5\ m$. (a) The compressed pulse output. (b) The peak power of compressed pulses vs. grating distance.

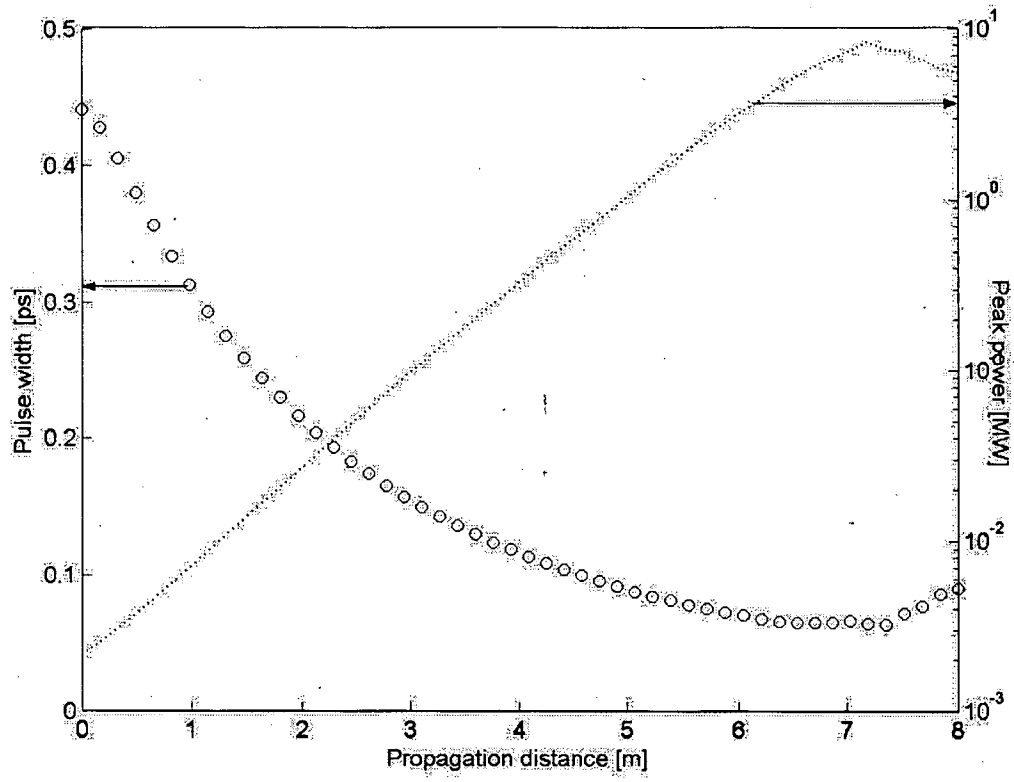

Fig. 5. Pulse compressor simulation results for the signal pulse vs. propagation distance. The peak powers of the compressed pulses are plotted (dotted line) with the corresponding pulse width (O mark).

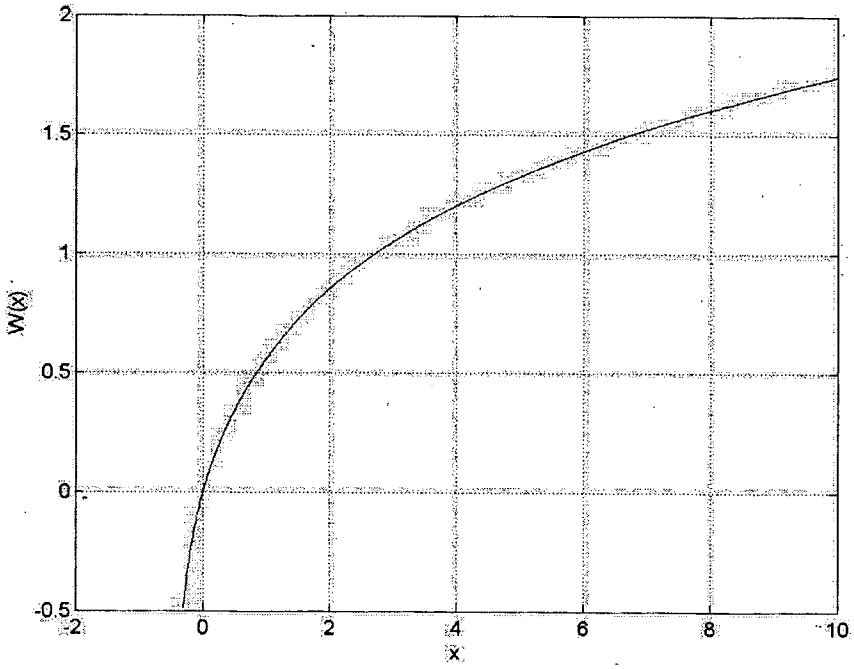

Fig. 6. Lambert W-function.